Understanding Interaction of Engineered Nanomaterials and Dissolved Organic Matters in River Sediments

Chen Zhang
Shanghai Municipal Engineering Design Institute Group Co Ltd
Xuejun Tan
Shanghai Municipal Engineering Design Institute Group Co Ltd
Xue Yang (yangxue@smedi.com)
Shanghai Municipal Engineering Design Institute Group Co Ltd

Research Article

Keywords: river sediments, titanium dioxide nanoparticles, dissolved organic matters, environmental behaviors, spectroscopy

Posted Date: March 7th, 2022

DOI: https://doi.org/10.21203/rs.3.rs-1359970/v1

Abstract

Engineered nanomaterials (ENMs) would be settled and accumulated in sediments beneath the surface water. Investigation on the interactions between ENMs and dissolved organic matters (DOM) in sediments could assist researchers in better understanding the environmental behaviors of ENMs. This study adopted heating methods to extract DOM from the sediments in a river of Shanghai, China, and titanium dioxide nanoparticles were used as model ENMs. Three-dimensional fluorescence spectra revealed that humic-like substances possessed a better binding ability with ENMs than protein-like substances and fatty acids. Nano-TiO_2 could destroy the α-helix structure of proteins. The rapidly diminishing intensity of α-helix bands suggested that secondary structure of protein was distorted, and the nano-TiO_2 binding site was amino residues in main peptide chain. X-ray photoelectron spectra further not only demonstrated that protein-like, humic-like substances and fatty acids could adsorb on the surface of nano-TiO_2, but also confirmed that phosphonate could combine with nano-TiO_2 via P-Ti covalent bond. This study supported comprehensively scientific data and assisted in understanding the environmental behaviors of ENMs, in order to direct the pollution control of river sediments.

1. Introduction

Nanoparticles (NPs) have attracted a great deal of interest because of their unique physicochemical and electrical properties. Engineered nanomaterials (ENMs) are intentionally produced or manufactured materials with at least one dimension between 1 and 100nm. At this size, materials behave differently to their bulk forms, which is of great interest for novel applications (Lewis et al., 2019; Pan and Xing 2012). For instance, silver nanoparticles are used in clothes and packaging. Titanium dioxide nanoparticles (nano-TiO_2) and zinc oxide nanoparticles (nano-ZnO) are applied in surface treatment and cosmetics. Graphene oxide and carbon nanotubes have applications in water treatment as new adsorbents (Suhendra et al., 2020). The increasing production and application of ENMs have resulted in their increasing release into the environment. It has been estimated that approximately 20,000 t of ENMs are expected to end up in municipal incineration facilities worldwide on an annual basis (Xu et al., 2019). Untreated ENMs may undergo a physical, chemical, and biological transformation, posing a serious threat to the ecological security of surface water and human health due to the inverse functions of target organs toxicity (Bai and Tang 2020; Welz et al., 2018). Overall, quantitatively characterizing the occurrence and potential bioavailability of ENMs in sediments is critical to better understand the fate and risks assessment of ENMs.

ENMs can enter sediments in aquatic environment through wastewater disposal, atmospheric deposition, or runoff discharge (Tou *et al.*, 2020). Sediments can act as a significant sink for multiple pollutants. As environmental conditions changes, the pollutants deposited in sediments can release to overlying water, causing secondary pollution incidents (Li et al., 2016). Dissolved organic matter is heterogeneous class of water-soluble compounds that contain organic carbon from animals, plants, and microbial metabolization, including humic acids, protein, carbohydrates, and other organics (Wang et al., 2016;

Zhang et al., 2011). DOM is a fundamental component of the aquatic active carbon cycle and plays a major role in the worldwide carbon cycle, nutrient export, and food chain (Lynch et al., 2019). In aquatic ecosystems, DOM and some hazardous pollutants (like heavy metal ions) can form complexes by the way of adsorption or complexation. After that, the fundamental characters of DOM would be changed, including bioavailability, migration, and transformation. Meanwhile, DOM has the potential to alter the bioavailability of other nutrients (like C, N, and P) as well as other biogeochemical processes (Li et al., 2014; Li et al., 2016). When ENMs enter sediments, DOM will have a direct impact on the migration and transformation of ENMs. Thus, it is necessary to investigate the interactions of DOM and ENMs so as to understand the environmental performances of ENMs (Philippe and Schaumann, 2014).

Previous studies mostly aimed at investigating interactions between the DOM of overlying water or a certain pure matter (like humic acid or fulvic acid) and ENMs. Based on the above studies, the adsorption, dispersion/aggregation or reduction/oxidation has been brought forward, which was basically determined by the types of DOM and ENMs (Philippe and Schaumann, 2014). As the most active matter in surface water, DOM components directly influence the substances migration and carbon cycle (Battin et al., 2009), ultimately causing different environmental performances. The components and concentrations of DOM in overlying water and in sediments are greatly different, and accordingly their reactivities are so different (Gueguen et al., 2012). Therefore, the interactions between DOM and ENMs would be of great reference value. Due to the heterogenous features of DOM, ultraviolet-visible spectroscopy (UV-VIS), fluorescence spectrum, size exclusion chromatography (SEC), nuclear magnetic resonance (NMR) and fourier-transform ion cyclotron resonance mass spectrometer (FT-ICR-MS) could be adopted to characterize the DOM (Chen et al., 2017). Furthermore, the fluorescence spectrum can quickly and precisely analyze DOM, so as to track the dynamic and geochemical processes of DOM (Fellman et al., 2010). Especially, three-dimensional excitation-emission matrix spectrofluorimetric(3D-EEM) can provide much more information about the molecular structure of DOM (Wang et al., 2009).

This study extracted DOM from actual river sediments and adopted nano-TiO_2 as the model of ENMs. Three-dimensional EEM, fourier transform infrared spectroscopy and X-ray technology were introduced to comprehensively investigate the interaction mechanisms between DOM and ENMs. Furthermore, the environmental behaviors of ENMs in river sediments could be brought up. This study could provide more scientific results for maintain ecological security of surface water.

2. Materials And Methods

2.1 Sampling and DOM extraction

Sediments were sampled from a river in Shanghai, China. The average sediments depth is 0.73m. The sediments (0–20 cm) were collected by core sampler, and then brought back to the laboratory in an ice box for vacuum drying. The DOM was further extracted according to reported method (Li et al., 2016). Specifically, the dried sediments were grinded and passed through a 100 mesh sieve, and 5g sample powder was then added into 1000 ml of ultra-pure water. Then, the mixture was shaken on the

thermostatic oscillator for 16 h at a temperature of 25 ℃ and a speed of 220 rpm. After shaking, the suspension was further centrifuged for 10 min at a speed of 10000 rpm, and then filtered through a membrane of 0.45 μm. DOM-contained filtrate was finally obtained.

2.2 Interactions between DOM and nano-TiO_2

The tests were carried out in brown reaction tubes in order to avoid the interference of photoreactions. Each reaction volume was set at 8 ml. Firstly, 4 ml of the above-extracted DOM solutions were added into 6 tubes, respectively. Secondly, 4 ml of nano-TiO_2 mixtures with the final concentrations of 0, 16, 32, 64, 128 mg/L was mixed. After thoroughly mixing, the mixtures reacted for 4 h at 25℃. Three-dimensional fluorescence spectra was applied to analyze the products. Moreover, the above experiments were repeated at 15 ℃ and 5 ℃ respectively to investigate the thermodynamic process.

2.3 Fitting of three-dimensional fluorescence spectra

The quenching constants of fluorescent groups can be calculated by Stern-Volmer equation (Eftink and Ghiron 1981):

$$F_0/F = 1 + K_{SV}Q = 1 + K_q\tau_0 Q \quad (2-1)$$

Where F_0 and F are the steady-state fluorescence intensities in the absence and presence of quenchers, K_q is quenching rate constant of the biological macromolecular, τ_0 is the average lifetime without any quenchers and the fluorescence lifetime of the biomacromolecules is 10^{-8} s (Lakowicz and Weber, 1973), Q is quencher concentration, K_{sv} is the Stern-Volumer quenching constant.

For static quenching, the binding constant (K_b) and the numbers of binding site number (n) can be determined by the following Eq. 2[1].

$$\lg((F_0-F)/F) = \lg K_b + n\lg(Q) \quad (2-2)$$

The thermodynamic parameters ΔS, ΔH and ΔG can be obtained by the following equation (Klotz and Urquhart, 1949).

$$\ln K_b = (-\Delta H/RT) + \Delta S/R \quad (2-3)$$

$$\Delta G = \Delta H - T\Delta S \quad (2-4)$$

Where R is the ideal gas constant (8.314 J/(mol·K)), T is the absolute temperature (K), and K is the distribution coefficient, the entropy change (ΔS) and enthalpy change (ΔH) can be determined from the slope and intercept of a plot of $1/T$ versus $\ln K_b$, and Gibbs free energy (ΔG) can be calculated from ΔH, ΔS and T by Eq. (4).

2.4 Analytical methods

Functional groups analysis were carried out on Fourier Transform Infrared Spectrometer (FTIR). The infrared spectra of protein were further analyzed in amide I region (1600–1700 cm^{-1}) to obtain the secondary structural information (Hou et al., 2015; Jiang et al., 2010). The excitation and emission wavelength was 200-550nm. Furthermore, the analytical method of 2D-COS from FTIR was referred to the literature reported by (Noda, 1989). Elemental analysis of nano-TiO_2 surface was carried out via monochromic AlKαX ray (Wang et al., 2020).

3. Results And Discussion

3.1 Interactions between different components of DOM and nano-TiO_2

Three-dimensional fluorescence spectra of DOM was as shown in Fig. 1. The excitation and emission wavelength represent different matters (Chen et al., 2003). Two typical fluorescent substances are respectively protein-like (excitation wavelength at 280 nm, emission wavelength at 342nm) and humic-like (excitation wavelength at 325 nm, emission wavelength at 412 nm) substances. Protein-like substances were generally autogenesis, which was derived from residues or metabolites of phytoplankton and bacteria. Marine humic-acid was originated from degradation or transformation of aquatic organics (Zhu et al., 2017).

After adding nano-TiO_2, quenching of two fluorescent matters of DOM was illustrated in Fig. 2. Fluorescence intensities of two DOM matters were synchronously decreased with the increasing nano-TiO_2 concentrations. As nano-TiO_2 concentration reached 128 mg/L, fluorescent signal strength of protein-like substances was decreased from 1586.7 to 827.2 (at 15°C), 981.1 (at 25°C) and 1128.7 (at 35°C), respectively. Meanwhile, fluorescent signal strength of humic-like substances was decreased from 404.9 to 331.0 (at 15°C), 351.6 (at 25°C) and 366.2 (at 35°C), respectively.

Fluorescence quenching represented intense interactions between nanoparticles and two predominant components of DOM. In the absence of nano-TiO_2, the maximum emission wavelength of protein-like and humic-like substances was 342nm and 410nm, respectively. After reacting with nano-TiO_2, the maximum emission wavelength of protein-like substances did not indicate obvious changes, and only about 1nm redshift was detected when the highest concentration of nano-TiO_2 (128mg/L) was added. Protein quenching was predominantly induced by conformational change or direct fluorescence quenching. The maximum emission wavelength was intimately influenced by the molecular structure and hydrophilicity/hydrophobicity of ambient micro-environment (Burstein et al., 1973; Quagraine et al., 2001). Redshift represented hydrophilic enhancement, while blueshift meant to be hydrophobic enhancement. As direct quenching reactions of two fluorophores (tryptophan and tyrosine) occurred, the molecular structure of reacted amino acid was accordingly and evidently changed. However, the two fluorophores (tryptophan and tyrosine) of un-reacted amino acid kept stable, and thus only the hydrophilicity of micro-environment was slightly increased.

Furthermore, maximum emission wavelength of humic-like substances was 410nm. After reacting with nano-TiO_2, the blueshift was detected, which could be enhanced with the increasing of nano-TiO_2 or the decreasing temperature. As the concentration of nano-TiO_2 reached 128mg/L, maximum wavelength was 400nm, 405nm and 406nm at the temperature of 15°C, 25°C and 35°C, respectively. It is suggested that the hydrophobicity of fluorophore was strengthened, and moreover the fluorescence intensity was decreased. It represented that the humic-like substances would be significantly changed.

3.2 Binding characters and process

3.2.1 Dynamic and static quenching

Excited-state reactions, energy transfer and ground-state complex formation lead to the decrease in fluorescence intensity of a fluorophore, including dynamic quenching and static quenching. As shown in Fig. 3 and table S1, the quenching rate constant K_q of Sten-volmer equation was calculated. The K_{sv} of protein-like substances at 15°C, 25°C and 35°C was respectively 5.58×10^{10} L/mol·s, 3.74×10^{10} L/mol·s and 2.48×10^{10} L/mol·s, which was higher than the maximum rate constant of dynamic quenching (2×10^{10} L/mol·s) (Ware, 1962). It was suggested that the static quenching was attributed to the complexation of protein-like substances and nano-TiO_2, while protein-like composites (tryptophan-like and tyrosine-like fluorophores) resulted in the decrease of fluorescence intensity (Bai et al., 2017). The K_{sv} of humic-like substances at 15°C, 25°C and 35°C was respectively 1.37×10^{10} L/mol·s, 0.98×10^{10} L/mol·s and 0.68×10^{10} L/mol·s. The K_{sv} values were lower than maximum rate constant of dynamic quenching. Higher temperature might enhance the rate of molecular motion, which further resulted in higher quenching rate. However, the K_{sv} value in this study was decreased with the increasing temperature, which was belong to the static quenching (Zhou et al., 2008). Hence, static quenching was ascribed to the complexation of humic-like substances and nano-TiO_2. Previous studies also approved that the interaction between nano-TiO_2 and anthraquinone substances could initiate static quenching (Pushpam et al., 2014). Phenolic group could cause the attachment of humic-acid substances, and smaller carboxyl groups also could set off complexation with nano-TiO_2 (Philippe and Schaumann, 2014).

3.2.2 Binding sites and binding properties

As to static quenching of protein-like and humic-like substances, binding site number and constant were illustrated in Fig. 4 and Table S2. Binding site number (n) was 0.8–0.9 for protein-like substances for nano-TiO_2. Consistent with this, the value of n was less than one in human serum albumin (HAS) for nano-TiO_2 (Ali et al., 2018). However, binding site number for humic-like substances was higher than one. The results suggested that lager binding ability and higher binding stability were prominent in the interaction of humic-like substance and nano-TiO_2. Binding constant (K_b) of protein-like and humic-like substances for nano-TiO_2 decreased from 213.65, 331.81 to 128.32, 244.12 with the decreasing temperature, respectively. It illustrated that low temperature could maintain the complex stability.

Thermodynamical parameters, including gibbs free energy change (ΔG), enthalpy change (ΔH) and entropy change (ΔS), were calculated according to van'Hoff equation (Eq. 2–3 and Eq. 2–4). These constants could assist in understanding the binding mechanisms of biomacromolecules and nano-TiO_2. The ΔG value of the interactive process of nano-TiO_2 and protein-like substance was − 12.74 KJ/mol, while − 14.40 KJ/mol for nano-TiO_2 and humic-like substance. Negative ΔG suggested good thermodynamic feasibility, which further represented the combination with nano-TiO_2 was spontaneous. The ΔH value of the interactive process of nano-TiO_2 and protein-like substance was − 18.69 KJ/mol, while − 11.64 KJ/mol for nano-TiO_2 and humic-like substance. Negative ΔH suggested that the reactions are exothermic. Therefore, decreasing temperature is beneficial for keeping the complex stability, which is accordance with Fig. 3. The ΔS value of the interactive process of nano-TiO_2 and protein-like substance was − 19.97 J/mol·K, while 9.27 J/mol·K for nano-TiO_2 and humic-like substance. When ΔH and ΔS are both lower than zero, the intermolecular forces are hydrogen bond and van der Waals force. When negative ΔH and positive ΔS are simultaneously presented, the predominant intermolecular force is controlled by electrostatic forces (Ma et al., 2016; Tunc et al., 2013). Based on these above, hydrogen bond and van der Waals force determined the combination of protein-like substances and nano-TiO_2 at 25°C. Previous study once found out that the combination of trypsin and nano-TiO_2 was determined by hydrogen bond and van der Waal force ((Momeni et al., 2017). Electrostatic forces controlled the combination of humic-like substances and nano-TiO_2. Considering the complexity of biomacromolecule's structure, protein and humic acid both possessed aromatic, hydrophilic, hydrophobic groups and binding cavities, which might exhibit noncovalent interaction (Gu et al., 2015). It also has been proved that the stable combination of lysozyme and nano-TiO_2 was not only dependent on hydrogen bonds but also controlled by noncovalent interaction (Xu et al., 2010).

3.3 Variations of functional moieties

FITR spectra of nano-TiO_2-DOM complex obtained under 25°C is shown in Fig. 5. Obvious variations of DOM structure were detected after nano-TiO_2 adsorption. The bands at ~ 2920 2850 cm^{-1} represent the emergence of asymmetric/symmetric C-H stretching of $-CH_2$ and $-CH_3$ (Wang et al., 2020). It demonstrated that fatty acids of DOM (in the absence of fluorophores) was react with nano-TiO_2. The bands at 1700 cm^{-1} and 1380 cm^{-1} were respectively assigned to the protonated carboxyl groups of DOM, which was speculated to be huimic-like substance. The band disappearance should be due to the complexation of -COOH and nano-TiO_2. The bands at 1600–1700 cm^{-1} was preferentially ascribed to the amid I that represented the secondary structure of protein. The secondary structure of protein with and without 128mg/L nano-TiO_2 was respectively shown in Fig. 5b and Fig. 5c. The DOM extracted from river sediment included aggregated strands, β-Sheet, α-Helix and 3-Turn helix with the content of 1.65%, 29.89%, 63.37% and 5.08. After the complexation with 128mg/L nano-TiO_2, the intensity of spectra bands decreased about on tenth, suggesting that the secondary structure of protein was distorted and amide I was severely damaged by nano-TiO_2 (Ranjan et al., 2016). Meanwhile, the content of each four primary secondary structure of protein respectively varied to 4.59%, 14.49%, 29.89% and 52.01%. Previous study

also reported that nano-TiO_2 could not only influence the content β-Sheet and α-Helix protein but also alleviate the transformation of these two protein (Ali et al., 2018; Momeni et al., 2017). The substantial reduction of α-Helix in DOM suggested that the nano-TiO_2 combined with the amino residues in primary peptide chain, and thus influence the content of α-Helix protein (Thakur et al., 2017).

2D-COS (Fig. 5d and Fig. 5e)could provide valuable information to untangle the complex reaction behaviors and to explain the associated mechanisms (Lee and Hur, 2016). As shown in synchronized spectrum (Fig. 5d), two diagonal bands at 2920 cm^{-1} and 2850 cm^{-1} represented fatty acids. The carboxyl groups of humic-like substances were claimed to be the bands at 1300cm^{-1} and 1700cm^{-1}. Amide I of protein-like substances was assigned to be the bands at 1600cm^{-1} and 1700cm^{-1}. The density of all the above-mentioned bands were positive and became stronger with the increase of Nano-TiO_2 concentration. In the synchronized spectrum, the cross peaks out of the diagonal represent that two different spectrum variables (x and y axis) are simultaneously changed. Positive and negative signals respectively represent the variations on same and opposite directions. At the same time, response order of functional groups could be speculated via asynchronous spectrum. If the cross peaks are both positive or negative in synchronized and asynchronous spectrum, the spectral change of one variable was earlier than another one (Noda, 1989). Therefore, the response order was as following: carboxyl groups of humic-like substances(1300 cm^{-1} and 1700cm^{-1}) > fatty acids(2920 cm^{-1} and 2850 cm^{-1}) > amide I of protein-like substances(1600cm^{-1} and 1700cm^{-1}).

3.4 XPS spectra

The XPS spectra of complex of nano-TiO_2 (128mg/L) and DOM at 25°C was shown in Fig. 6a. Comparing on the NIST database (http://srdata.nist.gov/xps/selEnergyType.aspx), the binding energy peaks at 133.52, 285.87, 401.35 and 531.88 eV were assigned to P2p, C1s, N1s, Ti2p and O1s. In the XPS spectrum of Ti2p, two components were presented in the Ti2p spectrum: $Ti2p_{1/2}$ (465.06, 464.97 and 464.88eV) and $Ti2p_{2/3}$ (459.58, 459.32 and 459.44 eV), indicating that Ti existed in the form of Ti^{4+} (Yin et al., 2020). Two components were presented in P2p spectrum, indicating that phosphonate in DOM existed in the form of P-Ti. The peaks located at ~283.8 eV, ~284.2 eV, ~285.3 eV, and ~287.2 eV are assigned to C=C, C–C, C–O, and C O, respectively (Wang et al., 2020). Abundant C-C and C-O were detected, suggesting that aliphatic compounds were heavily adsorbed on the surface of nano-TiO_2, also approving the results in Fig. 5. In XPS spectrum of P2p, two components were presented: aromatic N (~ 399.0eV) and peptide N (~ 400.4 eV) (Hua et al., 2018), suggesting that the chemical reaction of protein was firstly happened before adsorption on nano-TiO_2. Two components were presented in XPS spectrum of O1: C-O (~532.43 eV) and Ti-O (~ 529.63eV), which was in agreement with previous study (Yin et al., 2020). Generally, XPS spectra not only demonstrated that protein-like, humic-like substances and fatty acids could adsorb on the surface of nano-TiO_2, but also confirmed that phosphonate could combine with nano-TiO_2 via P-Ti covalent bond.

3.5 Mechanisms speculation

Increasing nanoparticles were discharged into aquatic ecosystem, the adsorption, complexation and transformation of nanoparticles have been aroused wide concern. Besides, the environmental behavior of nanoparticle is highly relied on the dissolved organic ligands (Xu et al., 2016). Diverse DOM in river sediment would deduce variable environmental response of nano-TiO_2. As shown in Fig. 6, the DOM in river sediment primarily contains fatty acids, protein-like and humic-like substances, which all could react with nano-TiO_2 and then adsorb on the surface of nanoparticles. The response order was as follow: humic-like substances > fatty acids > protein-like substances. The protein-like substances was mainly depended by hydrogen bond and van der Waals' forces, while the humic-like substances was primarily determined by electrostatic forces. The phosphonate was combined with nano-TiO_2 via P-Ti covalent bond. Tou et al., (2021) found that Ti-containing nanoparticles in estuary sediments were non-bioavailable, but these ENMs could be easily transformed into bioavailable form with the aid of DOM. Due to the DOM identified as the potential incentive, the results of this study promulgated the interactions between DOM and nano-TiO_2, which could alleviate the comprehension of Nano-TiO_2 environmental behaviors and direct the ecological risks control of nano-TiO_2.

4. Conclusion

Three primary DOMs in river sediment, including protein-like substances, humic-like substances and fatty acids, could react with nano-TiO_2. Furthermore, the humic-like substances revealed the strongest biding ability than the other DOMs. XPS spectra proved that the secondary structure of protein-like substances was damaged due to nano-TiO_2 addition. Hydrogen bond and van der Waals’ forces dominated the combination of protein-like substances and nano-TiO_2. Electrostatic forces controlled the combination of humic-like substances and ENMs. Meanwhile, phosphonate was combined with nano-TiO_2 via P-Ti covalent bond.

Declarations

Acknowledgement

This work is financially supported by Science and Technology Innovation Project of Shanghai (No. 21DZ2208700), Environmental protection science and technology research program of Shanghai (No.2021-25), and rising-star program of Shanghai Municipal Engineering Design Institute (Group) Co., LTD.(K2021K109).

Ethical Approval

Not applicable. The study has no data collected from human subjects.

Consent to Participate

All authors have agreed to participate this study.

Consent to Publish

All authors have approved and agreed to publish the paper in Environmental Science and Pollution Research.

Authors Contributions

Chen Zhang and Xuejun Tan designed research and analyzed data. Xue Yang developed the significance of the study and wrote the manuscript.

Competing Interests

None.

Availability of data and materials

Not applicable.

Declaration of Interest Statement

The authors declare that they have no known competing financial interests or personal relationships that could have appeared to influence the work reported in this manuscript.

References

1. Ali K, Abul Qais F, Dwivedi S, Abdel-Salam EM, Ansari SM, Saquib Q, Faisal M, Al-Khedhairy AA, Al-Shaeri M, Musarrat J (2018) Titanium dioxide nanoparticles preferentially bind in subdomains IB, IIA of HSA and minor groove of DNA. J Biomol Struct Dyn 36:2530–2542
2. Bai CC, Tang M (2020) Toxicological study of metal and metal oxide nanoparticles in zebrafish. J Appl Toxicol 40:37–63
3. Bai LL, Zhao Z, Wang CL, Wang CH, Liu X, Jiang HL (2017) Multi-spectroscopic investigation on the complexation of tetracycline with dissolved organic matter derived from algae and macrophyte. Chemosphere 187:421–429
4. Battin TJ, Luyssaert S, Kaplan LA, Aufdenkampe AK, Richter A, Tranvik LJ (2009) The boundless carbon cycle. Nat Geosci 2:598–600
5. Burstein E, Vedenkina N, Ivkova M (1973) Fluorescence and the location of tryptophan residues in protein molecules. Photochem Photobiol 18:263–279
6. Chen ML, Kim SH, Jung HJ, Hyun JH, Choi JH, Lee HJ, Huh IA, Hur J (2017) Dynamics of dissolved organic matter in riverine sediments affected by weir impoundments: Production, benthic flux, and environmental implications. Water Res 121:150–161
7. Chen W, Westerhoff P, Leenheer JA, Booksh K (2003) Fluorescence excitation - Emission matrix regional integration to quantify spectra for dissolved organic matter. Environ Sci Technol 37:5701–

5710

8. Eftink MR, Ghiron CA (1981) Fluorescence Quenching Studies with Proteins. Anal Biochem 114:199–227
9. Fellman JB, Hood E, Spencer RGM (2010) Fluorescence spectroscopy opens new windows into dissolved organic matter dynamics in freshwater ecosystems: A review. Limnol Oceanogr 55:2452–2462
10. Gu YL, Yin MX, Zhang HM, Wang YQ, Shi JH (2015) Study on the binding interaction of chromium(VI) with humic acid using UV-vis, fluorescence spectroscopy and molecular modeling. Spectrochim Acta A 136:1702–1709
11. Gueguen C, Burns DC, McDonald A, Ring B (2012) Structural and optical characterization of dissolved organic matter from the lower Athabasca River, Canada. Chemosphere 87:932–937
12. Hou XL, Liu ST, Zhang ZT (2015) Role of extracellular polymeric substance in determining the high aggregation ability of anammox sludge. Water Res 75:51–62
13. Hua B, Yang J, Liu FJ, Zhu GC, Deng BL, Mao JD (2018) Characterization of dissolved organic matter/nitrogen by fluorescence excitation-emission matrix spectroscopy and X-ray photoelectron spectroscopy for watershed management. Chemosphere 201:708–715
14. Jiang W, Yang K, Vachet RW, Xing BS (2010) Interaction between Oxide Nanoparticles and Biomolecules of the Bacterial Cell Envelope As Examined by Infrared Spectroscopy. Langmuir 26:18071–18077
15. Klotz IM, Urquhart JM (1949) The Binding of Organic Ions by Proteins - Effect of Temperature. J Am Chem Soc 71:847–852
16. Lakowicz JR, Weber G (1973) Quenching of Fluorescence by Oxygen - Probe for Structural Fluctuations in Macromolecules. Biochemistry-Us 12:4161–4170
17. Lee BM, Hur J (2016) Adsorption Behavior of Extracellular Polymeric Substances on Graphene Materials Explored by Fluorescence Spectroscopy and Two-Dimensional Fourier Transform Infrared Correlation Spectroscopy. Environ Sci Technol 50:7364–7372
18. Lewis RW, Bertsch PM, McNear DH (2019) Nanotoxicity of engineered nanomaterials (ENMs) to environmentally relevant beneficial soil bacteria - a critical review. Nanotoxicology 13:392–428
19. Li YP, Wang SR, Zhang L, Zhao HC, Jiao LX, Zhao YL, He XS (2014) Composition and spectroscopic characteristics of dissolved organic matter extracted from the sediment of Erhai Lake in China. J Soil Sediment 14:1599–1611
20. Li YP, Zhang L, Wang SR, Zhao HC, Zhang R (2016) Composition, structural characteristics and indication of water quality of dissolved organic matter in Dongting Lake sediments. Ecol Eng 97:370–380
21. Lynch LM, Sutfin NA, Fegel TS, Boot CM, Covino TP, Wallenstein MD (2019) River channel connectivity shifts metabolite composition and dissolved organic matter chemistry.Nat Commun10

22. Ma XL, Guo LQ, Wang Q, He JW, Li H (2016) Spectroscopy and Molecular Modeling Study on the Interaction Between Mycophenolate Mofetil and Pepsin. J Fluoresc 26:599–608
23. Momeni L, Shareghi B, Saboury AA, Evini M (2017) Interaction of TiO_2 nanoparticle with trypsin analyzed by kinetic and spectroscopic methods. Monatsh Chem 148:199–207
24. Noda I (1989) Two-Dimensional Infrared-Spectroscopy. J Am Chem Soc 111:8116–8118
25. Pan B, Xing BS (2012) Applications and implications of manufactured nanoparticles in soils: a review. Eur J Soil Sci 63:437–456
26. Philippe A, Schaumann GE (2014) Interactions of Dissolved Organic Matter with Natural and Engineered Inorganic Colloids: A Review. Environ Sci Technol 48:8946–8962
27. Pushpam S, Yamini D, Ramakrishnan V (2014) Luminescent Study of the Binding Interaction on 1,4-Dihydroxy-2,3-Dimethyl-9,10-Anthraquinone with Titanium Dioxide Nanoparticles.J Appl Spectrosc + 81,371–376
28. Quagraine EK, Kraatz HB, Reid RS (2001) Peptides mimicking the N-terminal Cu(II)-binding site of bovine serum albumin: synthesis, characterization and coordination with Cu(II) ions. J Inorg Biochem 85:23–32
29. Ranjan S, Dasgupta N, Srivastava P, Ramalingam C (2016) A spectroscopic study on interaction between bovine serum albumin and titanium dioxide nanoparticle synthesized from microwave-assisted hybrid chemical approach. J Photoch Photobio B 161:472–481
30. Suhendra E, Chang CH, Hou WC, Hsieh YC (2020) A Review on the Environmental Fate Models for Predicting the Distribution of Engineered Nanomaterials in Surface Waters.Int J Mol Sci21
31. Thakur S, Hashim N, Neogi S, Ray AK (2017) Size-dependent adsorption and conformational changes induced in bovine serum albumin (BSA) on exposure to titanium dioxide (TiO2) nanoparticles. Sep Sci Technol 52:421–434
32. Tou FY, Wu JY, Fu JQ, Niu ZS, Liu M, Yang Y (2021) Titanium and zinc-containing nanoparticles in estuarine sediments: Occurrence and their environmental implications. Sci Total Environ 754:142388
33. Tunc S, Cetinkaya A, Duman O (2013) Spectroscopic investigations of the interactions of tramadol hydrochloride and 5-azacytidine drugs with human serum albumin and human hemoglobin proteins. J Photochem Photobiology B-Biology 120:59–65
34. Wang Y, Zhang MM, Zhang D, Shen ZY (2016) The influence of sediment particle size on the properties of adsorbed dissolved organic matter in the Yangtze Estuary and its interactions with As/Sb. Mar Pollut Bull 105:351–358
35. Wang YL, Yang K, Lin DH (2020) Nanoparticulate zero valent iron interaction with dissolved organic matter impacts iron transformation and organic carbon stability. Environ Sci-Nano 7:1818–1830
36. Wang ZW, Wu ZC, Tang SJ (2009) Characterization of dissolved organic matter in a submerged membrane bioreactor by using three-dimensional excitation and emission matrix fluorescence spectroscopy. Water Res 43:1533–1540

37. Ware WR (1962) Oxygen quenching of fluorescence in solution: an experimental study of the diffusion process. J Phys Chem 66:455–458
38. Welz PJ, Khan N, Prins A (2018) The effect of biogenic and chemically manufactured silver nanoparticles on the benthic bacterial communities in river sediments. Sci Total Environ 644:1380–1390
39. Xu HC, Pan JZ, Zhang HH, Yang LY (2016) Interactions of metal oxide nanoparticles with extracellular polymeric substances (EPS) of algal aggregates in an eutrophic ecosystem. Ecol Eng 94:464–470
40. Xu P, Chen M, Lai C, Zeng GM, Huang DL, Wang H, Gong XM, Qin L, Liu YY, Mo D, Wen XF, Zhou CY, Wang RZ (2019) Effects of typical engineered nanomaterials on 4-nonylphenol degradation in river sediment: based on bacterial community and function analysis. Environ Sci-Nano 6:2171–2184
41. Xu Z, Liu XW, Ma YS, Gao HW (2010) Interaction of nano-TiO2 with lysozyme: insights into the enzyme toxicity of nanosized particles. Environ Sci Pollut R 17:798–806
42. Yin ZZ, Song L, Song HW, Hui K, Lin ZP, Wang Q, Xuan LL, Wang ZH, Gao WJ (2020) Remediation of copper contaminated sediments by granular activated carbon-supported titanium dioxide nanoparticles: Mechanism study and effect on enzyme activities. Sci Total Environ 741:139962
43. Zhang YL, Yin Y, Liu XH, Shi ZQ, Feng LQ, Liu ML, Zhu GW, Gong ZJ, Qin BQ (2011) Spatial-seasonal dynamics of chromophoric dissolved organic matter in Lake Taihu, a large eutrophic, shallow lake in China. Org Geochem 42:510–519
44. Zhang YZ, Dai J, Zhang XP, Yang X, Liu Y (2008) Studies of the interaction between Sudan I and bovine serum albumin by spectroscopic methods. J Mol Struct 888:152–159
45. Zhou QJ, Xiang JF, Tang YL, Liao JP, Yu CY, Zhang H, Li L, Yang YY, Xu GZ (2008) Investigation on the interaction between a heterocyclic aminal derivative, SBDC, and human serum albumin. Colloid Surf B 61:75–80
46. Zhu TB, Duan PF, He JG, Zhao MM, Li M (2017) Sources, composition, and spectroscopic characteristics of dissolved organic matter extracted from sediments in an anthropogenic-impacted river in Southeastern China. Environ Sci Pollut R 24:25431–25440

Figures

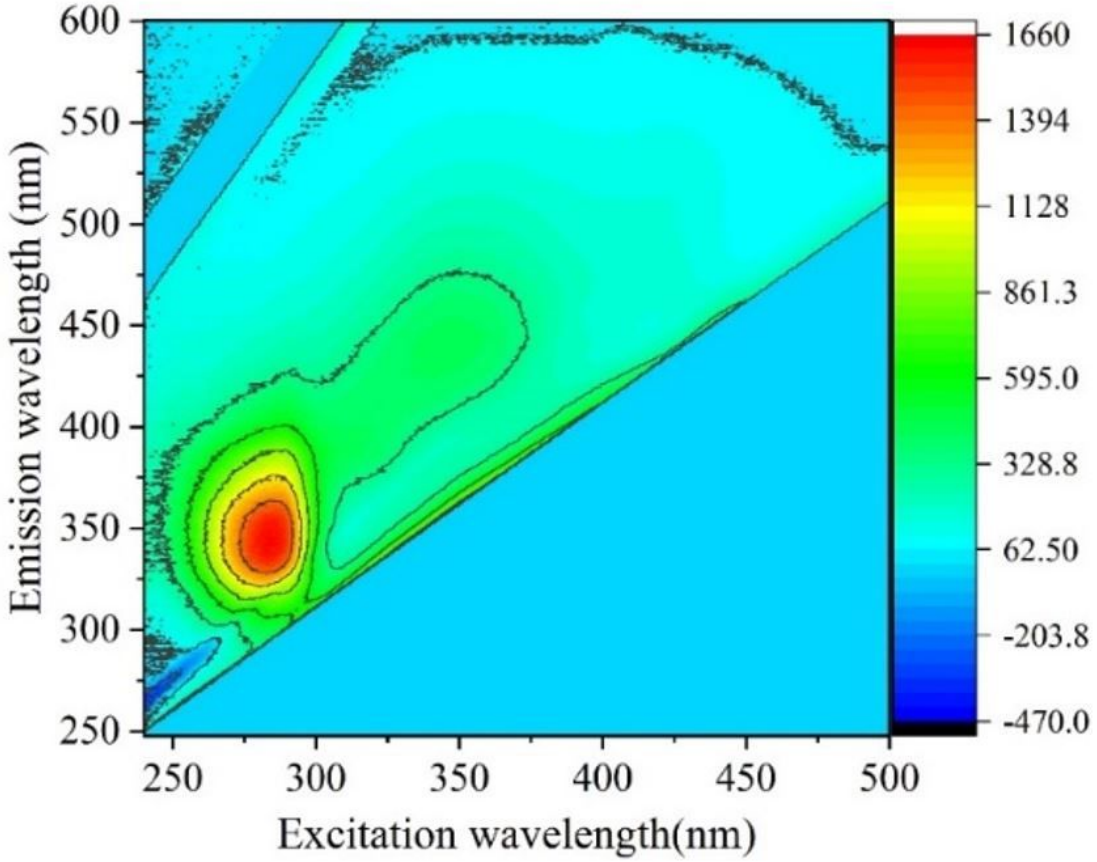

Figure 1

Three-dimensional fluorescence spectra of DOM.

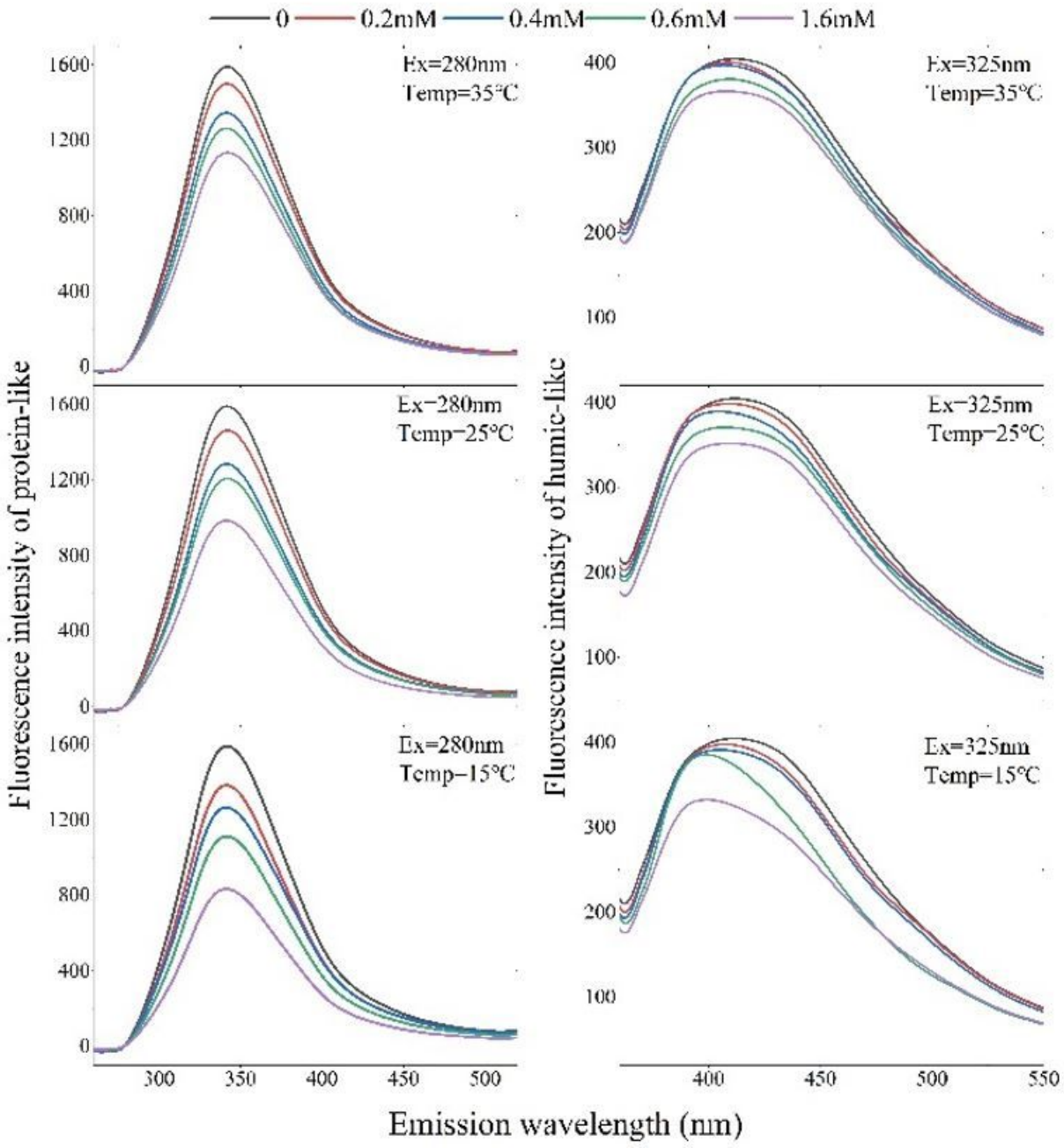

Figure 2

Fluorescence intensities of protein-like and humic-like substances.

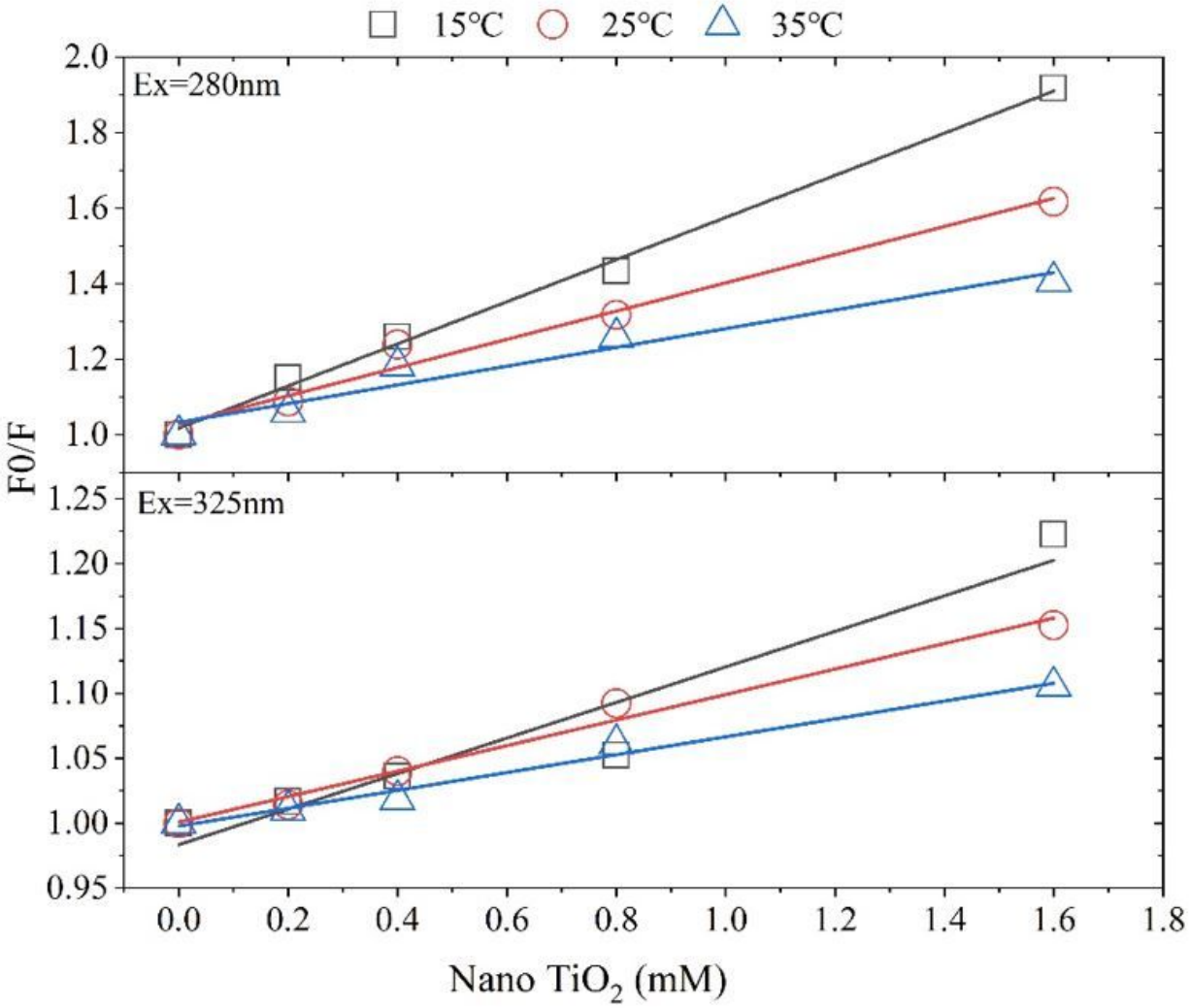

Figure 3

Fitted results of fluorescence spectra via SV formula.

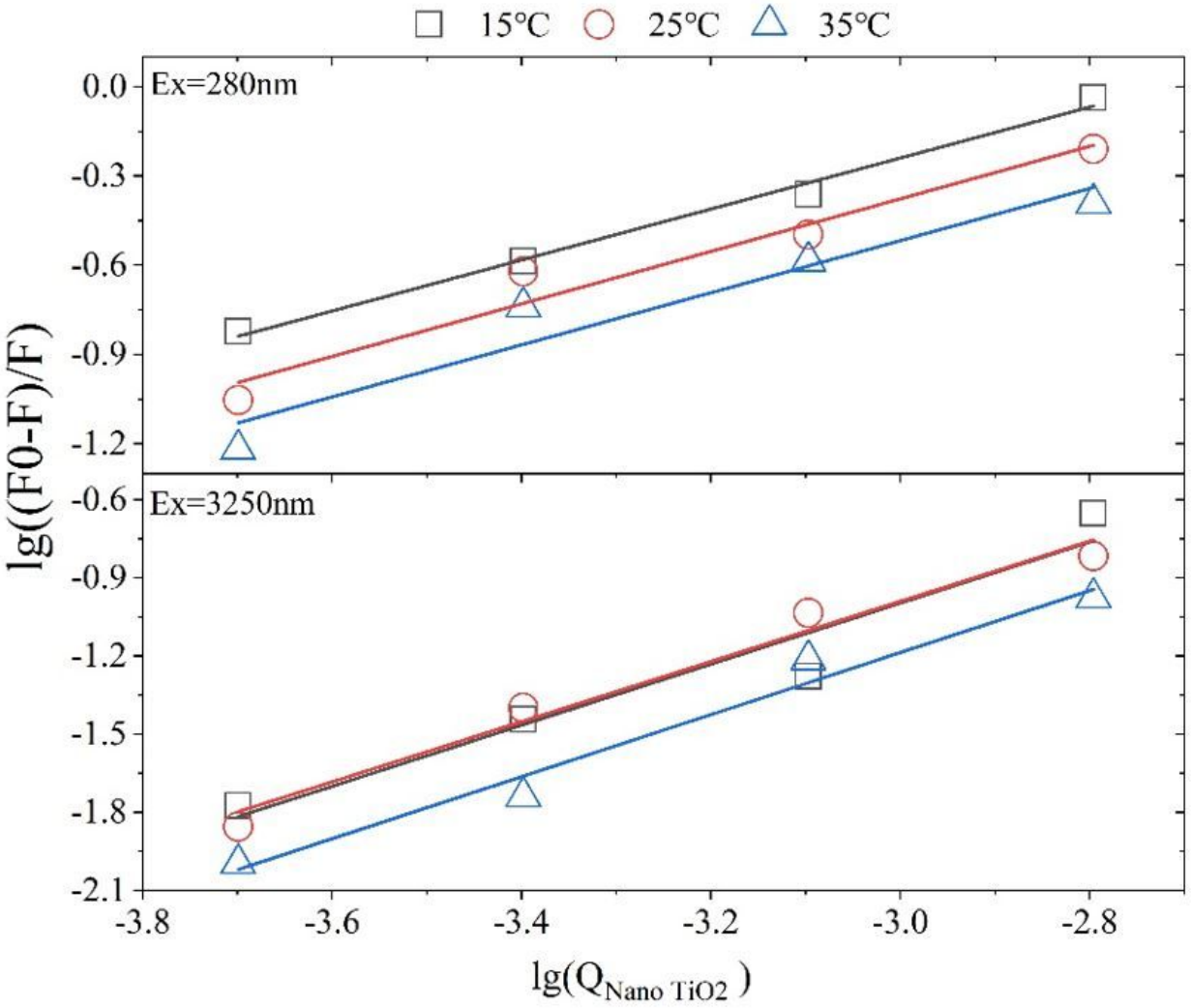

Figure 4

Double log plot for the quenching of protein-like and humic-like substances by nano-TiO_2

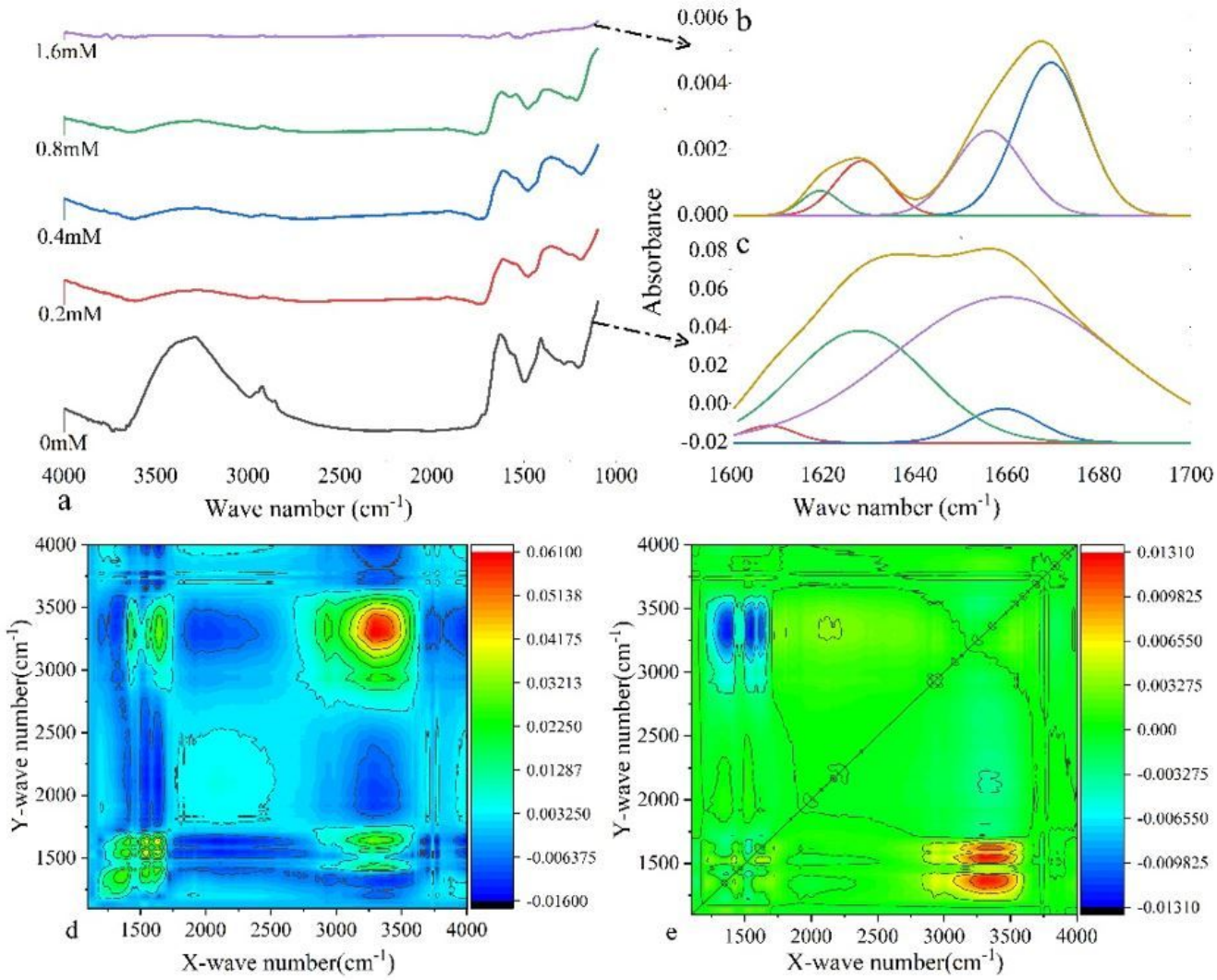

Figure 5

Fourier transform infrared spectra of complex of nano-TiO_2 and DOM.

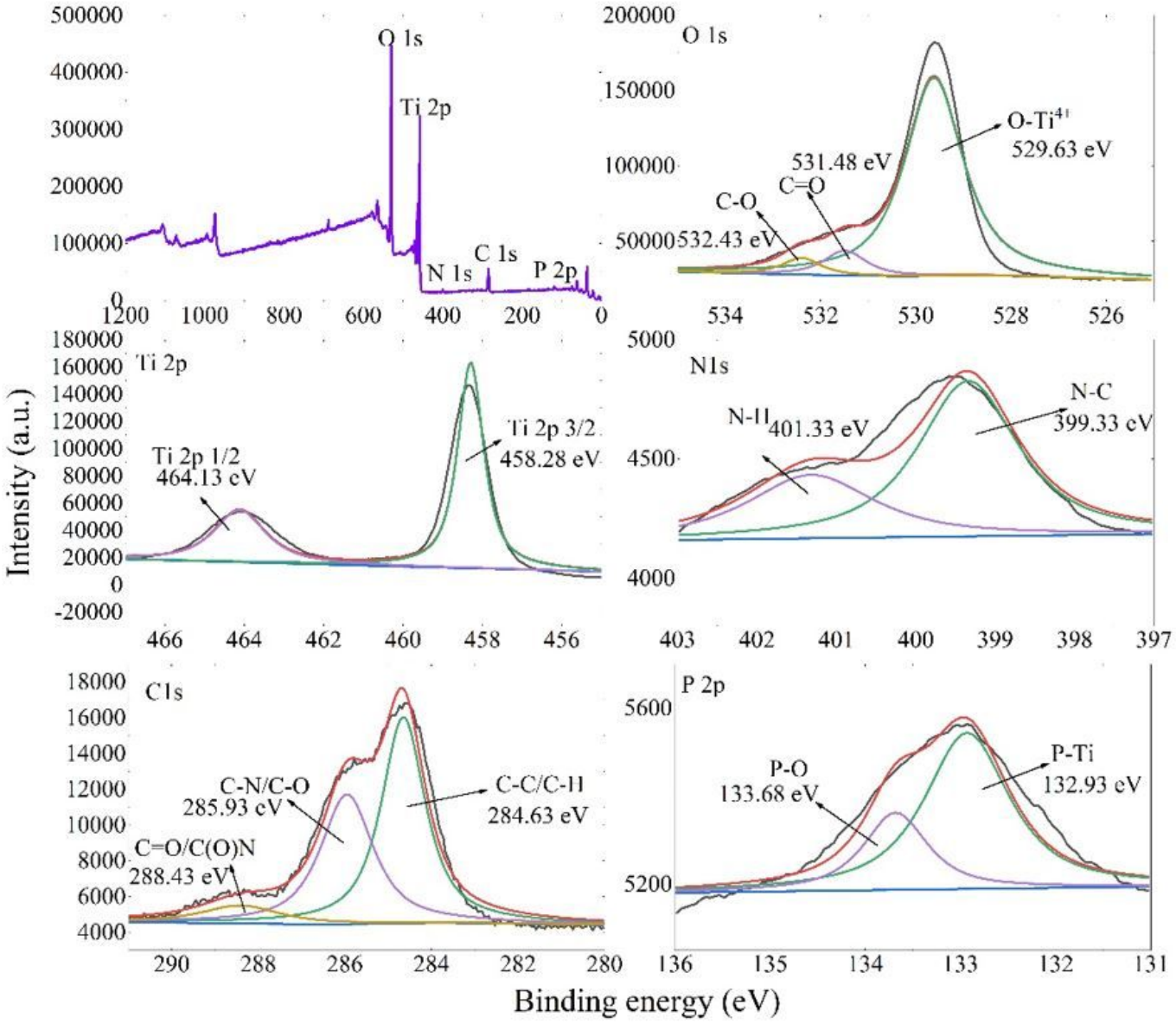

Figure 6

XPS spectra of complex of DOM and nano-TiO_2.

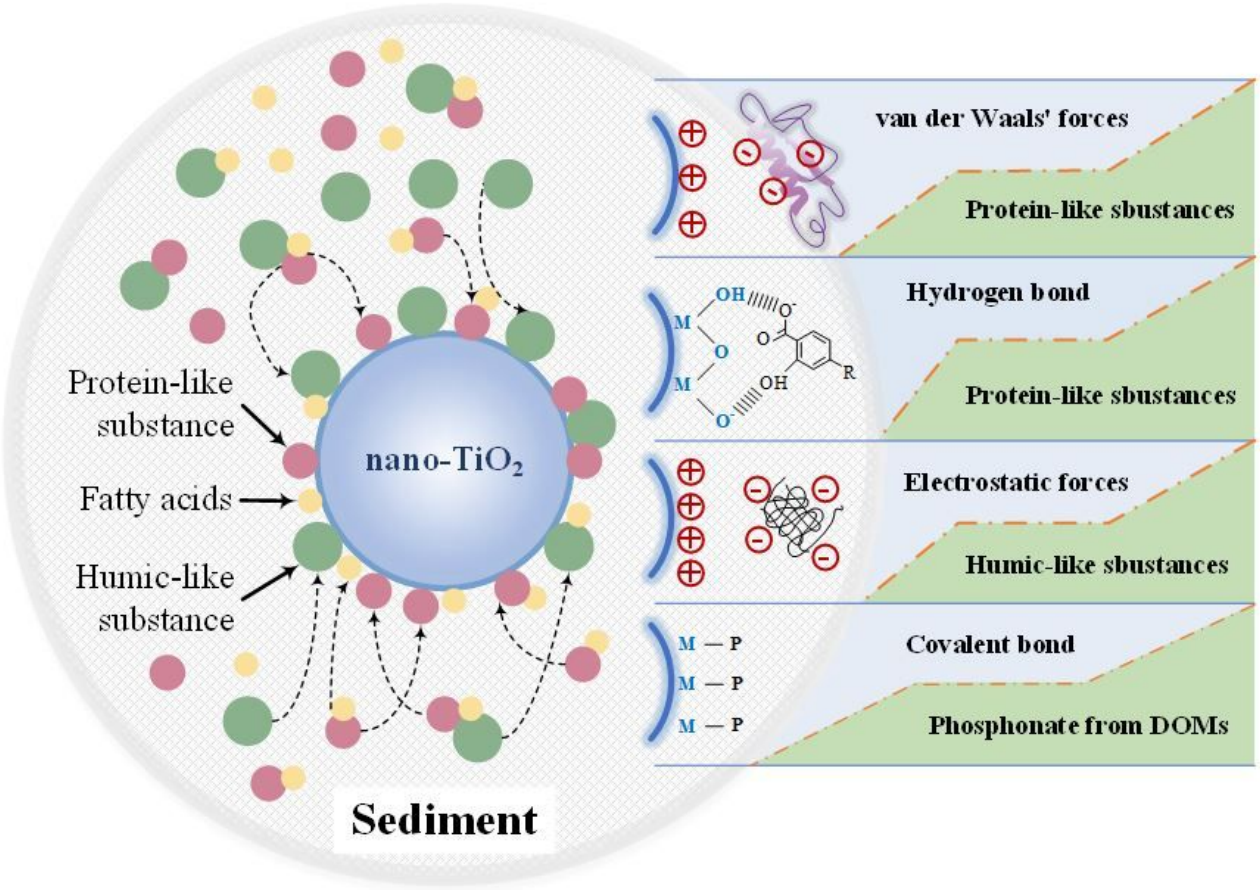

Figure 7

Schematic for the reaction mechanisms of sediments and nano-TiO_2.

Supplementary Files

This is a list of supplementary files associated with this preprint. Click to download.

- Supplementalfiles.docx